FRAMEWORK AND METHODOLOGY FOR RISK-BASED BRIDGE AND TUNNEL ASSET MANAGEMENT

Risk-based Asset Ranking and Corridor Prioritization

TECHNICAL REPORT DOCUMENTATION PAGE

1. Report No. https://archives.pdx.edu/ds/psu/44418	2. Government Accession No.	3. Recipient's Catalog No.
4. Title and Subtitle Framework and Methodology for Risk-Based Bridge and Tunnel Asset Management: Risk-Based Asset Ranking and Corridor Prioritization		5. Report Date November 10, 2025 6. Performing Organization Code:
7. Author(s) David Y. Yang (ORCID: 0000-0003-0959-6333) Arash Khosravifar (ORCID: 0000-0002-7137-6289) Diane Moug (ORCID: 0000-0001-5256-0438) Portland State University Avinash Unnikrishnan (ORCID: 0000-0001-6737-0485) University of Alabama at Birmingham		8. Performing Organization Report No.
9. Performing Organization Name and Address Portland State University Department of Civil and Environmental Engineering 1920 SW 4th Avenue, Office 301F Portland, OR 97201 DUNS: 052226800		10. Work Unit No. 11. Contract or Grant No. 693JJ321C000030
12. Sponsoring Agency Name and Address Office of Bridges and Structures Federal Highway Administration 1200 New Jersey Ave SE Washington, DC 20590		13. Type of Report and Period Final Report August 2024 - November 2025 14. Sponsoring Agency Code
15. Supplementary Notes		

16. Abstract

This report presents the results of Phase II of the project, "Framework and Methodology for Risk-based Bridge and Tunnel Asset Management". The research was carried out at Portland State University in collaboration with engineers and officials at the Oregon Department of Transportation (ODOT) and Federal Highway Administration (FHWA). Using the framework and methodology developed in Phase I of the project, the primary goal of Phase II is to showcase the practical application in risk-based asset management. In particular, the report includes the following two case studies: Case Study I — Weighted hazard scenarios for seismic risk assessment of Oregon Highway Bridges, and Case Study II — Accessibility risk assessment and corridor prioritization for Portland bridge network under a scenario Cascadia Subduction Zone (CSZ) earthquake. Each case study focuses on a specific method proposed in the Phase I of the project.

17. Key Words Objective asset risk assessment Performance risk of transportation networks Performance-based asset management	18. Distribution Statement No restrictions. This document is available to the public through the National Technical Information Service, Springfield, VA 22161. http://www.ntis.gov

19. Security Classif. (of this report) Unclassified	20. Security Classif. (of this page) Unclassified	21. No. of Pages 35	22. Price

Form DOT F 1700.7 (8-72) Reproduction of completed page authorized.

SI* (MODERN METRIC) CONVERSION FACTORS

APPROXIMATE CONVERSIONS TO SI UNITS

Symbol	When You Know	Multiply By	To Find	Symbol
		LENGTH		
in	inches	25.4	millimeters	mm
ft	feet	0.305	meters	m
yd	yards	0.914	meters	m
mi	miles	1.61	kilometers	km
		AREA		
in^2	square inches	645.2	square millimeters	mm^2
ft^2	square feet	0.093	square meters	m^2
yd^2	square yard	0.836	square meters	m^2
ac	acres	0.405	hectares	ha
mi^2	square miles	2.59	square kilometers	km^2
		VOLUME		
fl oz	fluid ounces	29.57	milliliters	mL
gal	gallons	3.785	liters	L
ft^3	cubic feet	0.028	cubic meters	m^3
yd^3	cubic yards	0.765	cubic meters	m^3
		NOTE: volumes greater than 1000 L shall be shown in m^3		
		MASS		
oz	ounces	28.35	grams	g
lb	pounds	0.454	kilograms	kg
T	short tons (2000 lb)	0.907	megagrams (or "metric ton")	Mg (or "t")
		TEMPERATURE (exact degrees)		
^oF	Fahrenheit	5 (F-32)/9 or (F-32)/1.8	Celsius	^oC
		ILLUMINATION		
fc	foot-candles	10.76	lux	lx
fl	foot-Lamberts	3.426	candela/m^2	cd/m^2
		FORCE and PRESSURE or STRESS		
lbf	poundforce	4.45	newtons	N
lbf/in^2	poundforce per square inch	6.89	kilopascals	kPa

APPROXIMATE CONVERSIONS FROM SI UNITS

Symbol	When You Know	Multiply By	To Find	Symbol
		LENGTH		
mm	millimeters	0.039	inches	in
m	meters	3.28	feet	ft
m	meters	1.09	yards	yd
km	kilometers	0.621	miles	mi
		AREA		
mm^2	square millimeters	0.0016	square inches	in^2
m^2	square meters	10.764	square feet	ft^2
m^2	square meters	1.195	square yards	yd^2
ha	hectares	2.47	acres	ac
km^2	square kilometers	0.386	square miles	mi^2
		VOLUME		
mL	milliliters	0.034	fluid ounces	fl oz
L	liters	0.264	gallons	gal
m^3	cubic meters	35.314	cubic feet	ft^3
m^3	cubic meters	1.307	cubic yards	yd^3
		MASS		
g	grams	0.035	ounces	oz
kg	kilograms	2.202	pounds	lb
Mg (or "t")	megagrams (or "metric ton")	1.103	short tons (2000 lb)	T
		TEMPERATURE (exact degrees)		
^oC	Celsius	1.8C+32	Fahrenheit	^oF
		ILLUMINATION		
lx	lux	0.0929	foot-candles	fc
cd/m^2	candela/m^2	0.2919	foot-Lamberts	fl
		FORCE and PRESSURE or STRESS		
N	newtons	0.225	poundforce	lbf
kPa	kilopascals	0.145	poundforce per square inch	lbf/in^2

TABLE OF CONTENTS

LIST OF FIGURES

LIST OF TABLES

LIST OF ABBREVIATIONS AND SYMBOLS

BMS	bridge management system
CSZ	Cascadia Subduction Zone
DS	damage state
FHWA	Federal Highway Administration
FEMA	Federal Emergency Management Agency
IM	intensity measure
NBI	National Bridge Inventory
ODOT	Oregon Department of Transportation
PGA	peak ground acceleration
Sa	spectral acceleration
TMCMC	transitional Markov chain Monte Carlo
USGS	United States Geological Survey
A_{NET}	network accessibility index
$B_{p,k}$	benefit of project p for link k
$cq(ds)$	consequence associated with a DS
d	distance between a site and a fault in kilometers
$DS\|IM$	random variable representing DS conditioned on IM
IM	random variable representing IM of an adverse event
im_i	IM in the ith hazard scenario
M	magnitude of an earthquake
$p_{DS\|IM}$	probability of a specific DS conditioned on a specific IM level
$p(\mathbf{s})$	probability of a system state **s**
p_k and C_k	failure probability and indirect consequence associated with link k
w_i	responsibility weight of the ith hazard scenario
α_k	risk-informed importance measure of link k

β	reliability index
λ_{IM}	annual rate of exceedance for IM
$\mathcal{B}$	set of bridges
$\mathcal{G}$	graph model
$\mathcal{P}$	set of population nodes
$\mathcal{H}$	set of hospital nodes
$\mathcal{V}$ and $\mathcal{E}$	nodes and links in a graph

FRAMEWORK AND METHODOLOGY FOR RISK-BASED BRIDGE AND TUNNEL ASSET MANAGEMENT: RISK-BASED ASSET RANKING AND CORRIDOR PRIORITIZATION

EXECUTIVE SUMMARY

This report presents the results of Phase II of the project, "Framework and Methodology for Risk-based Bridge and Tunnel Asset Management". The research was carried out at Portland State University in collaboration with engineers and officials at the Oregon Department of Transportation (ODOT) and Federal Highway Administration (FHWA). Using the framework and methodology developed in Phase I of the project, the primary goal of Phase II is to showcase the practical application in risk-based asset management. In particular, the report includes the following two case studies:

- Case Study I: Weighted hazard scenarios for seismic risk assessment of Oregon Highway Bridges
- Case Study II: Accessibility risk assessment and corridor prioritization for Portland bridge network under a scenario Cascadia Subduction Zone (CSZ) earthquake

Each case study focuses on a specific method proposed in the Phase I of the project.

WEIGHTED SEISMIC HAZARD SCENARIOS OF OREGON HIGHWAY BRIDGES

Case study I demonstrated the applicability and scalability of the weighted hazard scenario method proposed in Phase I in state-level risk assessment endeavors. Specifically, the direct seismic risks of all 2,608 bridges owned by the Oregon Department of Transportation (ODOT) were analyzed. Their corresponding hazard scenarios were determined, including their return periods (annual rates), intensity measure values, direct failure consequences, and scenario weights. Table E.1 presents an example of the weighted risk table for one of the bridges. Risk is expressed in damaged deck area, which is commonly used to approximate direct repair costs. This table can be directly embedded into existing bridge manage processes. In addition, Figure E.1 shows top ranked bridges in terms of damaged deck area and damage ratio (damaged deck area over total deck area).

Table E.1. Risk Table of an example bridge (deck area = 104,005 m^2).

Hazard scenario	Description (return period, Sa)	Annual rate	Consequence (damage ratio)	Weight	Risk (m^2)
1	58.65-yr, Sa=0.075g	2.722×10^{-1}	4.990×10^{-4}	0.1846	2.609
2	477.9-yr, Sa=0.376g	8.293×10^{-3}	0.1962	0.4138	70.04
3	2312-yr, Sa=0.890g	1.102×10^{-3}	0.6795	0.6066	47.25
4	10491-yr, Sa=1.571g	1.890×10^{-4}	0.9129	0.7455	13.36
5	43795-yr, Sa=2.359g	3.830×10^{-5}	0.9776	0.8182	3.190
6	163025-yr, Sa=3.183g	9.430×10^{-6}	0.9936	0.8182	0.7977
7	536803-yr, Sa=3.971g	2.780×10^{-6}	0.9978	0.7455	0.2153
8	1474357-yr, Sa=4.652g	1.000×10^{-6}	0.9990	0.6066	0.0630
9	3135343-yr, Sa=5.166g	4.667×10^{-7}	0.9995	0.4138	0.02006
10	4866205-yr, Sa=5.468g	2.990×10^{-7}	0.9996	0.1846	0.005740
				Total risk	137.5

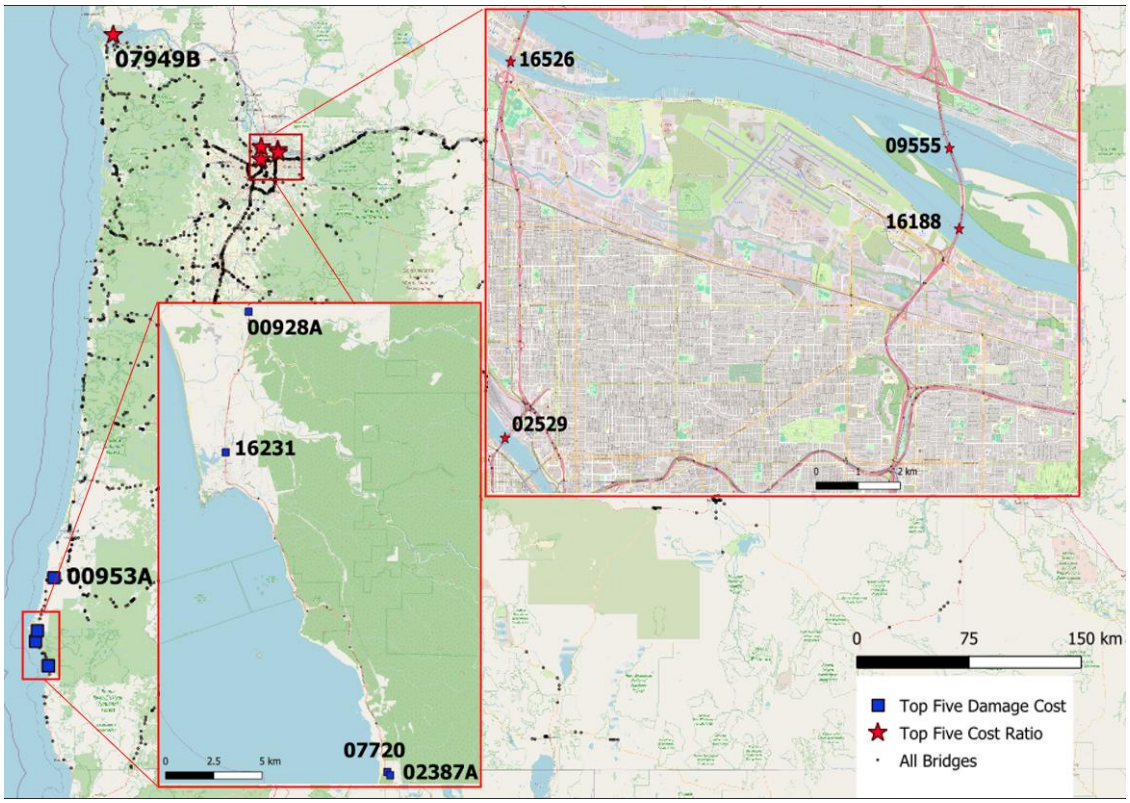

Source: FHWA; Base Map: Esri World Street Map

Figure E.1. Illustration. Locations of top five high-risk bridges in terms of deck area (representing damage cost) and damage ratio (representing cost ratio to replacing the asset). The first 5 to 6 digits of the full structure number is used as bridge ID.

CORRIDORS CRITICAL TO ACCESSIBILITY RISK OF PORTLAND BRIDGE NETWORK

Case study II focused on the indirect risk assessment using the transitional Markov chain Monte Carlo (TMCMC) approach proposed in Phase I. The assets under consideration were 644 bridges

located in the Portland metro area. The indirect risk was considered based on the accessibility to the regional hospitals immediately after a magnitude 9 CSZ earthquake scenario and quantified with an adapted Hansen accessibility index. The TMCMC-based sampling approach provided an efficient means of evaluating this indirect risk without exhaustively enumerating all possible failure combinations. It also yielded criticality of each link within the transportation network, as shown in Figure E.2. The criticality and the formulated importance measures thereafter offer a rational basis for retrofitting prioritization.

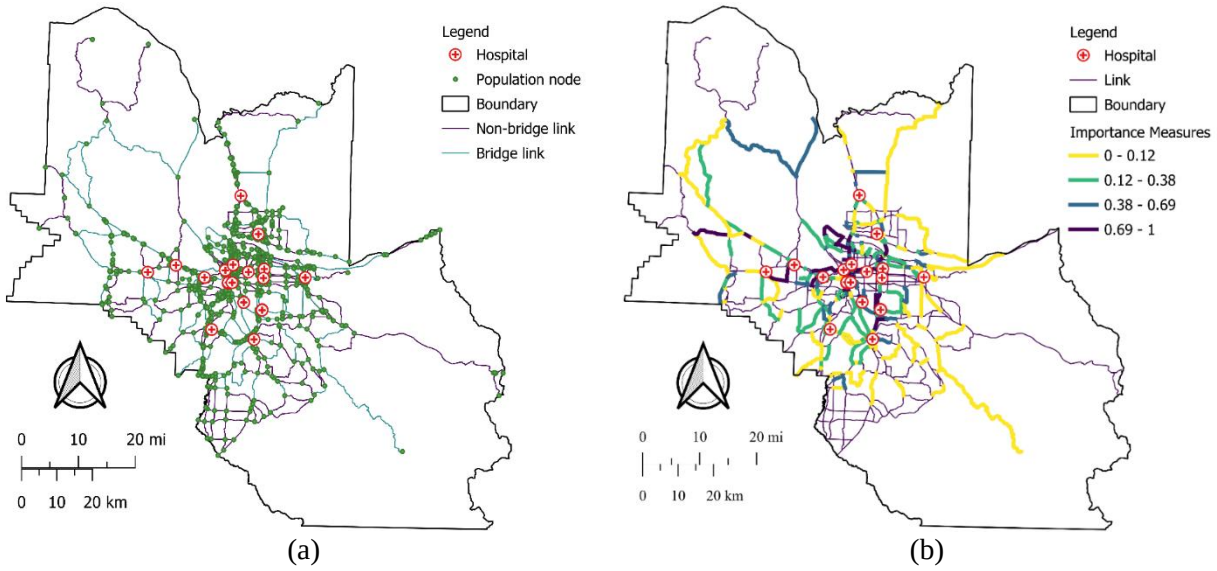

Source: FHWA

Figure E.2. Illustration. (a) Indirect risk: accessibility to hospitals and (b) risk-informed corridor criticality to hospital accessibility.

CHAPTER 1

WEIGHTED HAZARD SCENARIOS FOR SEISMIC RISK ASSESSMENT OF OREGON HIGHWAY BRIDGES

1.1 INTRODUCTION

This case study demonstrates the use of the weighted hazard scenario method for state-level risk assessment. Using the proposed method, the case study analyzed the seismic risk of all Oregon highway bridges owned by the Oregon Department of Transportation (ODOT). For each bridge, the hazard curve was obtained from United State Geological Survey (USGS), the bridge characteristics from the Federal Highway Administration (FHWA) InfoBridge database, and the fragility parameters from the HAZUS technical manual (FEMA, 2020). Based on these inputs, weighted hazard scenarios were developed and presented in a tabular format for potential integration with bridge management systems. The high-risk bridges were also identified.

Additionally, the case study addressed practical challenges related to the application of the weighted hazard scenario method, including

- How to incorporate hazard curves described by discrete data points of intensity measures and probabilities of exceedance in the USGS hazard model;
- The impact of the number of hazard scenarios on the accuracy of the estimated risk;
- How to determine whether the upper bound used in a risk integral is sufficient for accurate risk assessment.

Investigations on these questions and the results from the case study are presented in the following sections. To ensure the document is self-contained, the weighted hazard scenario approach is briefly reviewed, and more details of this approach can be found in the Phase I final report (Yang et al., 2024).

1.2 REVIEW OF WEIGHTED HAZARD SCENARIO METHOD

Applying the Gaussian quadrature to the risk integral yields the following expression:

$$R = \int_{im=a}^{im=b} \left[\sum_{ds} cq(ds) \cdot p_{DS|IM}(ds|im) \right] |\lambda_{IM}{}'(im)| dim$$
$$\approx \sum_{i=1}^{n} \underbrace{w_i}_{weight} \cdot \underbrace{\left[\sum_{ds} cq(ds) \cdot p_{DS|IM}(ds|im_i) \right]}_{expected\ consequence} \cdot \underbrace{v_{IM}(im_i)}_{nominal\ rate}$$

Equation 1.1. Risk calculation with numerical integration (Gaussian quadrature).

where a, b = lower and upper bound of the risk integral in terms of intensity measure (IM) values; $cq(ds)$ = average consequence given the damage state DS equal to ds; $p_{DS|IM}(ds|im_i)$ = probability of DS equal to ds given the IM equal to im; $\lambda_{IM}{}'(im)$ = gradient of the hazard curve

given the IM equal to im; $v_{IM}(im_i)$ = nominal rate of a hazard scenario; w_i = weight of the ith scenario event, equal to the integration weight η_i of the ith Gaussian integration point.

Equation 1.1 gives rise to n scenario events, each with a unique IM value im_i and responsibility weight w_i. For each scenario, the nominal annual rate of occurrence, $v_{IM}(im_i)$, is calculated as follows:

$$v_{IM}(im_i) = \frac{b-a}{2}|\lambda_{IM}{}'(im)|$$

Equation 1.2. Nominal annual rate of occurrence.

1.3 INCORPORATING DISCRETE HAZARD CURVES

As shown Equation 1.1, risk assessment with the weighted hazard scenarios calls for the likelihood values at specified IM values determined at Gaussian integration points, i.e., $\lambda_{IM}{}'(im)$. For a hazard curve with a closed-form expression, e.g., the fictitious hazard curve considered in the Phase I report, the hazard likelihood can be determined in a straightforward manner by taking the derivative of the closed-form hazard curve with respect to the IM. However, hazard curves in practice are often determined by a set of discrete IM values and their corresponding annual rates of exceedance. One notable example is the hazard curve provided by the USGS, which uses 20 pairs of IM values and the corresponding probabilities of exceedance to describe the probabilistic seismic hazard at a site (USGS, 2024).

This discrete format of hazard curves poses two challenges to the application of the proposed approach:

- First, the number of data points (e.g., 20 in the case of USGS data) may not be sufficient to derive the hazard likelihood. Additionally, the IM values of these data points are not evenly spaced, which can compromise the effectiveness of numerical differentiation.
- Second, even though the likelihood can be evaluated numerically at the discrete IM values, the integration points of a Gaussian quadrature do not necessarily overlap with the data points used to determine the hazard curve. Therefore, another step is needed to determine the hazard likelihood with respect to an IM value between the discrete values of a hazard curve.

Before applying the weighted hazard approach, the error associated with a discrete hazard curve is first investigated herein by re-visiting the analytical example presented in the Phase I report. This closed-form hazard curve is presented as follows:

$$\overline{ln\,PGA} = -0.152 + 0.859M - 1.803\,ln(d+25)$$
$$\lambda_{IM}(im) = 1 - \Phi\left(\frac{ln\,im - \overline{ln\,PGA}}{\sigma}\right)$$

Equation 1.3. An analytical hazard curve.

where M = magnitude of the earthquakes generated at the fault ($M = 6.5$ in the Phase I example); d = distance between the site and the fault in kilometers ($d = 10$ km in the Phase I example); Φ = cumulative distribution function (CDF) of a standard normal distribution; σ = dispersion factor of the peak ground acceleration (PGA) at the site, i.e., the standard deviation of the logarithmic PGA, and $\sigma = 0.57$ is assumed herein (Cornell et al., 1979).

Herein, this closed-form hazard curve is discretized using IM values organized in a similar format to that of a USGS hazard curve, i.e., spaced as a geometric sequence. Two cases are considered. In Case I, 10 PGA values are selected within the integration domain and spaced as a geometric sequence (i.e., 0.0645g, 0.0954g, 0.1411g, …, 1.4785g, and 2.187g). In Case II, 20 PGA values are generated in a similar fashion (i.e., 0.0645g, 0.0776g, 0.0935g, …, 1.8168g, and 2.187g). In both cases, the corresponding annual rate of exceedance is calculated using Equation 1.3 and combined with the PGA value to form a data point on a discrete hazard curve. To obtain hazard likelihood from a discrete hazard curve, the following approximation strategies are explored and compared:

- Strategy I: Use the central difference method to estimate the likelihood values at the discrete PGA values; use linear interpolation between these discrete likelihood values to determine the likelihood at a specific PGA value used in the Gaussian quadrature.
- Strategy II: Conduct cubic spline interpolation between the logarithmic PGA values and the logarithmic rates of exceedance; Based on the gradient of the interpolated curve, the likelihood values at a specific PGA can be obtained as follows:

$$\lambda_{IM}(im) = -\frac{d\, v_{IM}(im)}{d \ln v_{IM}(im)} \cdot \frac{d \ln v_{IM}(im)}{d \ln im} \cdot \frac{d \ln im}{d\, im} = -\frac{f_{int}(\ln im)}{im} \cdot f_{int}{}'(\ln im)$$

Equation 1.4. Likelihood from cubic spline in log-log space.

  where f_{int} and $f_{int}{}'$ = interpolated function between $\ln im$ and $\ln v_{IM}(im)$ and its derivative, respectively.
- Strategy III: assume a linear relationship between the logarithmic PGA values and the logarithmic rates of exceedance (Sewell et al., 1991); based on linear regression results in the log-log scale, the hazard likelihood at a specific PGA can be expressed as

$$\lambda_{IM}(im) = -c \cdot k \cdot im^{k-1}$$

Equation 1.5. Likelihood from linear regression in log-log space.

  where c and k = intercept and slope, respectively, from the linear regression between $\ln im$ and $\ln v_{IM}(im)$.
- Strategy IV: assume a hyperbolic relationship between the logarithmic PGA values and the logarithmic rates of exceedance (Bradley et al., 2007); based on nonlinear regression results in the log-log scale, the hazard likelihood at a specific PGA can be expressed as

$$\lambda_{IM}(im) = \frac{exp\left(\frac{\alpha}{\ln im - s_{IM}} + s_{rate}\right)}{im} \cdot \frac{\alpha}{(\ln im - s_{IM})^2}$$

Equation 1.6. Likelihood from hyperbolic regression in log-log space.

where α, s_{rate}, and s_{IM} = model parameters for a hyperbolic model as determined in Bradley et al. (2007). They can be obtained with maximum likelihood estimation.

Strategies I and II do not rely on any parametric assumptions between the annual rate and the IM, while Strategies III and IV assume different parametric forms for the relationship. By setting the number of hazard scenarios to six (the same number used in the Phase I study), the seismic risk in the previous example is computed using the proposed approach and each of the four strategies described above. The results are presented in Table 1.1 together with the errors in the estimated risks relative to the benchmark value (which was computed in the Phase I study using numerical integration). In the Phase I study, the closed-form hazard curve in Equation 1.3 and its analytical derivatives were also used to determine the precise value of the risk integral. Table 1.1 indicates that regardless the number of data points, Strategies III and IV, which have been traditionally used in seismic design, cannot provide accurate risk estimates using the risk table approach. Nonetheless, it should be recognized that the parametric assumptions may be more robust to potential outliers and errors within the data. Both Strategies I and II are able to accurately estimate the risk when more data points are available (as in Case II). In Case I, however, Strategy I is no longer effective due to the limited data availability causing errors in numerical differentiation and linear interpolation. Across all strategies and both cases, Strategy II can deliver reasonable risk estimates. Therefore, Strategy II is used in the following analysis.

Table 1.1. Effectiveness of different strategies to handle discrete hazard curves.

Strategy	Case I Risk (damage ratio)	Case I Error (%)	Case II Risk (damage ratio)	Case II Error (%)
I	0.004258	28.24	0.003550	6.921
II	0.003400	2.403	0.003400	2.413
III	0.001635	–50.75	0.001783	46.29
IV	0.002696	–18.80	0.002754	–17.04

1.4 SEISMIC RISK OF OREGON HIGHWAY BRIDGES

1.4.1 Data Sources for Statewide Analysis

The proposed approach is applied to assess seismic risk for highway bridges in Oregon. The analysis utilizes site- and structure-specific data collected from public databases. Relevant information about highway bridges in Oregon is obtained from the InfoBridge database managed by the FHWA (FHWA, 2024a). All bridge types in the database are considered except for bridge-sized culverts, which are excluded by checking whether the field of the culvert condition rating is populated. In total, 2,608 bridges are analyzed for the seismic risk using the weighted hazard scenario method.

Hazard curves at the bridge sites are obtained from the USGS website (USGS, 2024) based on (a) the geospatial coordinates of a bridge (retrieved from the InfoBridge database) and (b) the soil class at the bridge site as determined by the National Earthquake Hazards Reduction Program (NEHRP) (NEHRP, 2020). The latter is publicly available as a GIS layer from the Oregon Department of Geology and Mineral Industries (DOGAMI, 2013). As mentioned previously, a USGS hazard curve is depicted by 20 discrete data points. Each data point includes a set of IMs and an annual rate of exceedance associated with the IM set. Following HAZUS (FEMA, 2020), the spectral acceleration (Sa) at 1 second is treated as the IM for bridge seismic risk assessment. For this IM, the hazard curve is depicted by a geometric sequence of 20 Sa values ranging from 0.0025g to 5.54g, which are also used as the lower and upper bound of the integration domain of the risk integral.

For structural vulnerability, the seismic fragility curves developed for HAZUS (FEMA, 2020) are adopted. All bridge characteristics necessary to the fragility analysis can also be obtained from the InfoBridge database. These characteristics include the year of construction, main span material, main span design, number of spans, length of maximum span, span length, and skew angle. It should be noted that other fragility models can certainly be used if the data can be gathered for all bridges under consideration.

In the analytical example in Task 2, the consequence associated with a DS is expressed as a damage ratio, i.e. ratio of repair cost to replacement cost, and the ratios are obtained from the HAZUS model (FEMA, 2020). In the case study herein, the same HAZUS damage ratios are considered for different DSs. However, to compare the risks of different bridges, the risk of a bridge is ultimately measured by the expected repair cost without normalization. To this end, the replacement cost of a bridge is proxied by the total deck area following previous studies (e.g., Dong and Frangopol, 2015; Padgett et al., 2010). As a result, the seismic risk of a bridge has the same unit as the deck area. The deck area information is collected from the InfoBridge database. The risk values in terms of the deck area can be readily monetized to reveal funding needs or for use in downstream optimization procedures. For example, an agency's average replacement cost estimates for a square foot can be multiplied with the risk values, or if bridge replacement unit costs differ by factors such as bridge type and locations, individual replacement unit costs can be applied to individual bridges.

It is noted that the ranking is influenced by the HAZUS fragility models used for vulnerability assessment, deck area records in the InfoBridge database, and the suitability of using deck area to proxy damage consequences. For instance, the deck area in the InfoBridge database is simply computed by multiplying the field of structure length and the field of the deck width. This may undercount the deck area in double-decker bridges. The consequences based on deck area may also miss the importance of a bridge in a route or the importance to daily traffic.

1.4.2 Determination of Weighted Hazard Scenarios

Given the diversity of bridge types and hazard characteristics, the investigation herein focuses on two aspects related to the determination of weighted hazard scenarios, including

- The number of hazard scenarios needed to analyze bridges with high seismic risks;
- The adequacy of upper-bound intensities provided in the USGS hazard curves.

For the weighted hazard scenario method, increasing the number of hazard scenarios can improve the accuracy of risk assessment. However, to practically implement the approach, it is essential to use a relatively small number of scenarios. Therefore, a balance should be maintained between achieving sufficient accuracy and ensuring feasibility for implementation. In the Phase I study, this was accomplished by (a) monitoring the change in the estimated risk as additional scenarios (i.e., integration points) were considered and (b) utilizing the set of scenarios if the change by adding another scenario fell below a certain threshold. Specifically, the previous analysis started with 4 scenarios and used a threshold of 5% to stop adding more scenarios. In the current investigation, this empirical termination criterion is first used to assess and rank the seismic risks of all bridges. To further examine this empirical termination criterion, a convergence study is performed for the five bridges with the highest seismic risks.

Figure 1.1 illustrates the variation in the estimated risk as the number of scenarios increases from 2 to 25. This range extends well beyond the point where the termination criterion (5%) is reached. Note that the bridge number used in the figure is the first five to six digits of the structure number recorded in the InfoBridge database. Their full structural numbers are 09555 064 02632, 16188 064 02525, 07949B009 00028, 16526 001 30759, and 02529 061 00332. Figure 1.1 indicates that for Bridges 09555 and 07949B, the empirical termination criterion used in the Phase I study may yield estimates different (by over 5%) from the more accurate risk estimates obtained with more scenarios. This discrepancy stems from the premature stopping when an inaccurate risk estimate does not vary for a few iterations. The error in risk estimation causes an incorrect ranking for Bridge 07949B, which should be placed as the third most critical bridge instead of the second. Despite the slight error in risk estimates and the swapped rankings between Bridges 07949B and 16188, the analysis with the original termination criterion is still able to identify the correct set of top-five most critical bridges.

To improve the convergence performance, more robust termination criteria could be devised, e.g., by using a greater increment when raising the scenario number, and/or by adopting a “patience” parameter (Géron, 2019) to consider a broader range of risk estimates before termination (rather than only two consecutive estimates). Alternatively, convergence studies similar to that in Figure 1.1 can be carried out to refine the risk estimates iteratively. In the following analysis, 10 scenarios are used to accurately estimate risks. This is because the risk estimates stabilize after 10 scenarios, indicating that further increasing scenario numbers only yields negligible improvements in accuracy.

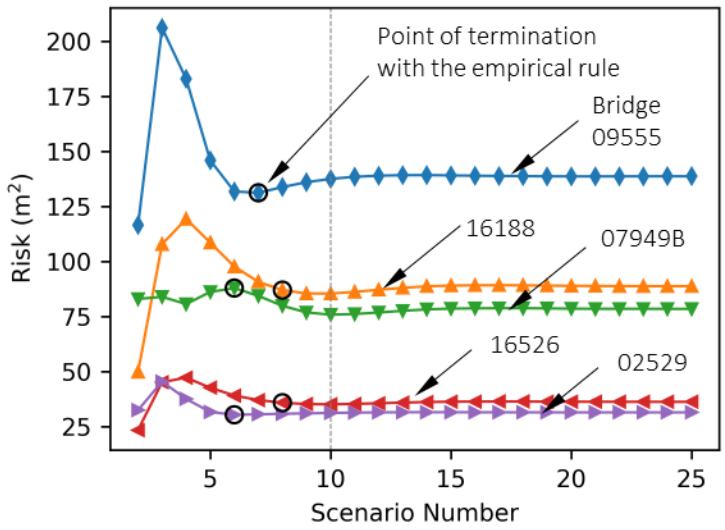

Source: FHWA

Figure 1.1. Graph. Estimated risk with increasing numbers of scenarios for the top five bridges with the highest seismic risk.

Apart from the scenario numbers, the accuracy of the estimated risk also depends on the upper bound of the integration domain, namely, how extreme of an IM value should be included in the risk integral. If the upper bound of the integration domain is too low, the seismic risk may be underestimated regardless of what risk assessment methods are used. The USGS hazard curves cover Sa values up to 5.54g. This upper bound is examined herein to check if it is sufficient to accurately estimate the seismic risk. To this end, the proposed approach is applied repetitively by incrementally increasing the upper bounds from 0.144g to 5.54g. Practically, this process starts with using the first 11 (out of 20) data points of the USGS hazard curve for risk assessment. In subsequent analysis, the datapoint with the next lowest Sa value in the unused data points is added to the hazard curve until all 20 data points are used in the analysis. The change in the estimated risk is tracked and plotted in Figure 1.2 for the top five bridges analyzed earlier. Following the previous discussion, 10 scenarios are used to tabulate the risk values. Figure 1.2 demonstrates that the increase in the estimated risk becomes marginal or negligible after Sa=2.4623g. This is due to the already high probability of collapse (complete damage state) at this intensity level. This also indicates that the upper bound of 5.54g available through USGS is sufficient to accurately assess the seismic risk.

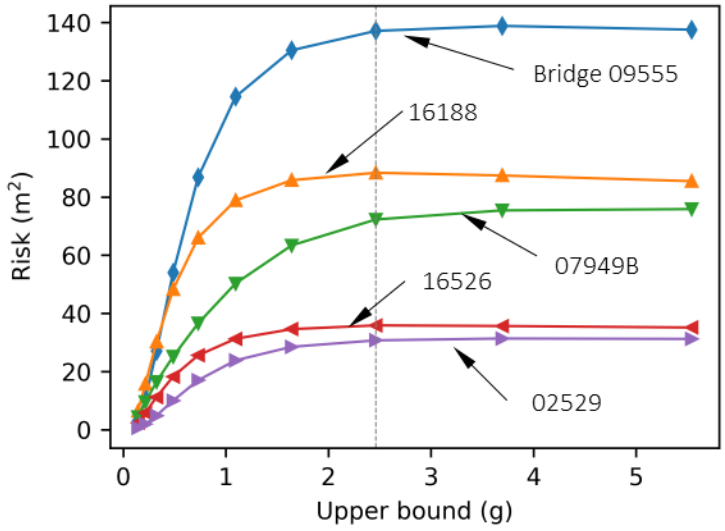

Source: FHWA

Figure 1.2. Graph. Estimated risk with gradually increased upper bounds.

1.4.3 Results of Seismic Risk Assessment

Based on the previous discussion, the seismic risks of all 2,608 highway bridges are assessed using the proposed approach with 10 hazard scenarios and an upper bound of Sa=5.54g. Table 1.2 presents the risk table for Bridge 09555 as an example, which, with a total deck area of 104,005 m^2, yields the highest seismic risk. Table 1.3 provides additional information for all top-five bridges analyzed previously. Figure 1.3 shows the locations of the top five bridges with the highest seismic risks. For comparison, the five bridges with the highest damage ratio are also highlighted in Figure 1.3. These bridges are expected to lose the largest fractions of their values due to seismic damage. It can be seen that the two sets of bridges do not overlap geographically. Bridges located on the southwest coast of Oregon and on poor soil conditions (e.g., Class E/F) are expected to sustain more severe seismic damage. However, larger bridges crossing the Columbia River have higher seismic risks, as approximated by deck areas, although their damage ratios are relatively low. It appears that seismic risks measured by repair cost (and approximated by deck area) favor larger bridges, which are usually located on major corridors or serving urban areas in the case study region. As a result, ranking bridges based on this indicator may cause biases against rural and remote communities. However, the relationship between larger bridges and their locations, albeit common due to higher traffic demand, may not always be the case across different regions. On the other hand, although more costly to repair, a larger bridge with a low damage ratio may have a shorter time to restore functionality compared to a smaller bridge with a high damage ratio (which may need replacement). Hence, the rankings based on repair cost may not well reflect risks. One reasonable approach for more comprehensive decision-making is to convert the risk in term of damage ratio to a utility value through a calibrated utility function (Goodwin and Wright, 2014; Keeney and Raiffa, 1993).

Table 1.2. Risk Table of Bridge 09555 (Deck area = 104,005 m^2).

Hazard scenario	Description (return period, Sa)	Annual rate	Consequence (damage ratio)	Weight	Risk (m^2)
1	58.65-yr, Sa=0.075g	2.722×10^{-1}	4.990×10^{-4}	0.1846	2.609
2	477.9-yr, Sa=0.376g	8.293×10^{-3}	0.1962	0.4138	70.04
3	2312-yr, Sa=0.890g	1.102×10^{-3}	0.6795	0.6066	47.25
4	10491-yr, Sa=1.571g	1.890×10^{-4}	0.9129	0.7455	13.36
5	43795-yr, Sa=2.359g	3.830×10^{-5}	0.9776	0.8182	3.190
6	163025-yr, Sa=3.183g	9.430×10^{-6}	0.9936	0.8182	0.7977
7	536803-yr, Sa=3.971g	2.780×10^{-6}	0.9978	0.7455	0.2153
8	1474357-yr, Sa=4.652g	1.000×10^{-6}	0.9990	0.6066	0.0630
9	3135343-yr, Sa=5.166g	4.667×10^{-7}	0.9995	0.4138	0.02006
10	4866205-yr, Sa=5.468g	2.990×10^{-7}	0.9996	0.1846	0.005740
			Total risk		137.5

Table 1.3. Information of the top five bridges with the highest seismic risk.

Structure Number	Longitude (degree)	Latitude (degree)	Risk (damage ratio)	Deck Area (m^2)	Risk (m^2)
09555	–122.548	45.5917	0.001323	104005	137.5
16188	–122.545	45.5768	0.002169	39404	85.46
07949B	–123.872	46.2361	0.002200	34479	75.87
16526	–122.681	45.6077	0.001938	18135	35.15
02529	–122.683	45.5381	0.001041	30002	31.23

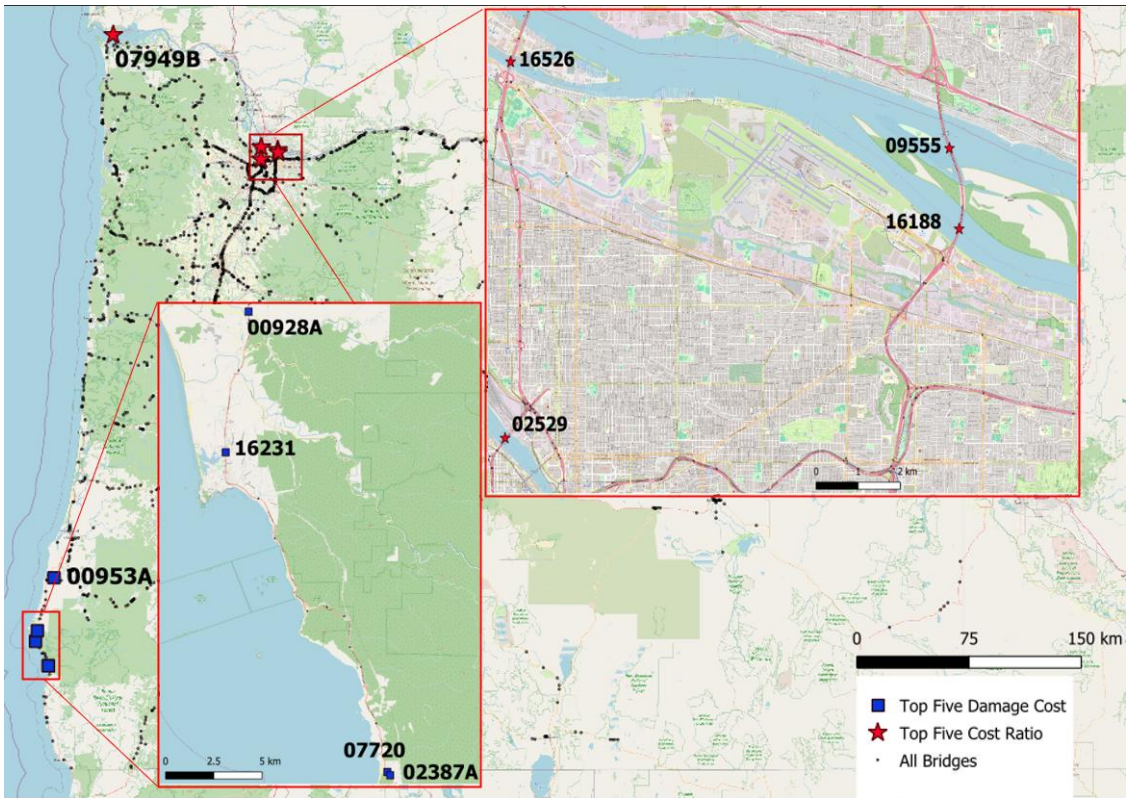

Source: FHWA; Basemap: Esri World Street Map

Figure 1.3. Illustration. Locations of top five bridges ranked by seismic risk (approximated with deck area) and top five bridges ranked by damage ratio (the first 5 to 6 digits of the full structure number is used for presentation clarity).

1.5 SUMMARY AND REMARKS

Case study I demonstrated the applicability and scalability of the weighted hazard scenario method. It is shown that the proposed method can support portfolio-level risk assessment at the scale of state highway networks. To ensure consistency and objectivity, it is essential to clearly document and reach consensus on the hazard model, fragility curves, and damage consequences used in the analysis. The hazard curve, fragility parameters, and weighted scenarios for all Oregon bridges are preserved in the PI's online drive and will be available upon reasonable request.

CHAPTER 2

MOBILITY RISK ASSESSMENT FOR LARGE-SCALE TRANSPORTATION NETWORKS

2.1 INTRODUCTION

Apart from the direct risk assessed at each individual bridge, performance indicators such as network connectivity, efficiency, flow capacity, and travel cost have also been employed in indirect risk assessment to evaluate the functionality and vulnerability of transportation networks under extreme events (Rivera-Royero et al., 2022). Quantifying risk using performance indicators means evaluating both the damage probability and the consequence of the entire system. For large-scale networks, the number of possible scenarios grows exponentially with the number of assets. This makes full enumeration considering all different failure/damage patterns computationally infeasible. In addition, system failure patterns with low probability but high consequences are likely to be missed by conventional Monte Carlo approaches, resulting in underestimated risk. To address this, Phase I study proposed the Transitional Markov Chain Monte Carlo (TMCMC) method (Yang et al., 2024). By leveraging TMCMC, both network-level risk and the importance of an asset to the overall risk can be efficiently determined, even for large-scale transportation networks.

Case Study II of this project focused on the demonstration of the TMCMC approach to accessibility risk assessment and risk-based corridor prioritization from the risk assessment results. The study investigated the accessibility risk of the transportation network in the Portland Metro Area, quantified based on the Hansen accessibility index from neighborhoods to the local hospitals under the anticipated Cascadia Subduction Zone earthquakes. In the aftermath of earthquakes, accessibility to critical services such as hospitals is a decisive measure of the network's performance in supporting emergency response and recovery efforts. It is shown from this case study that how such risks can inform the ranking and programming of retrofit measures.

2.2 NETWORK RISK ASSESSMENT OF TRANSPORTATION SYSTEMS

2.2.1 Graph Model of the Case Study Transportation Network

In this study, the network is constructed from primary arterial roads and designated emergency response routes in the Portland Metro Area, providing a representative system for assessing post-disaster accessibility. This setting offers a relevant context to examine how seismic events can disrupt connectivity and reduce access to critical services such as hospitals. This transportation network is modeled as a graph, expressed as follows:

$$\mathcal{G} = (\mathcal{V}, \mathcal{E})$$

Equation 2.1. Representation of a graph model.

where $\mathcal{V}$ = the set of nodes representing intersections, and $\mathcal{E}$ = the set of links representing road segments between these nodes. Some of these links contain one or more bridges, which are the primary vulnerable elements in the network and referred to herein as bridge links. Note that the

terms “network” and “graph” are used interchangeably in this study. For the purposes of accessibility assessment, nodes in the graph are further classified into two subsets: (1) the subset of population nodes, $\mathcal{P}$, consisting of nodes nearest to one or more census tract centroids, and (2) the subset of hospital nodes, $\mathcal{H}$, consisting of nodes nearest to one or more hospitals. The proximity is determined based on the geodesic distance, because the centroids and hospital locations normally do not coincide with the network nodes (thus making computing network distance impossible). Some network nodes may be closest to both a hospital and a census tract centroid. In this case, the accessibility of the census tract to the hospital reduces to the accessibility of a network node to itself, which cannot be reasonably estimated with the network model. Hence, whenever such cases arise, the accessibility of a node to itself is excluded from the calculation of accessibility.

To create the graph model, primary arterial roads and designated emergency response routes were extracted from the GIS data hosted by the Oregon Metro (Oregon Metro, 2025). The resulting network consists of 1,756 nodes and 2,639 links. Overall, the study area has 664 bridges. Bridges are assigned to links based on spatial alignment between bridge locations and road segments in the network. Among all 2,639 links, 461 links include one or more bridges, referred to herein as bridge links or bridge corridors. The network also includes 18 hospital nodes corresponding to the region’s healthcare facilities and 614 population nodes aggregating populations in communities across 1,619 census tracts. Since multiple census tracts may be mapped to the same nearest node, the number of population nodes is smaller than the number of tracts. Figure 2.1 shows the constructed network and the spatial distribution of bridge links, population nodes, and hospital nodes.

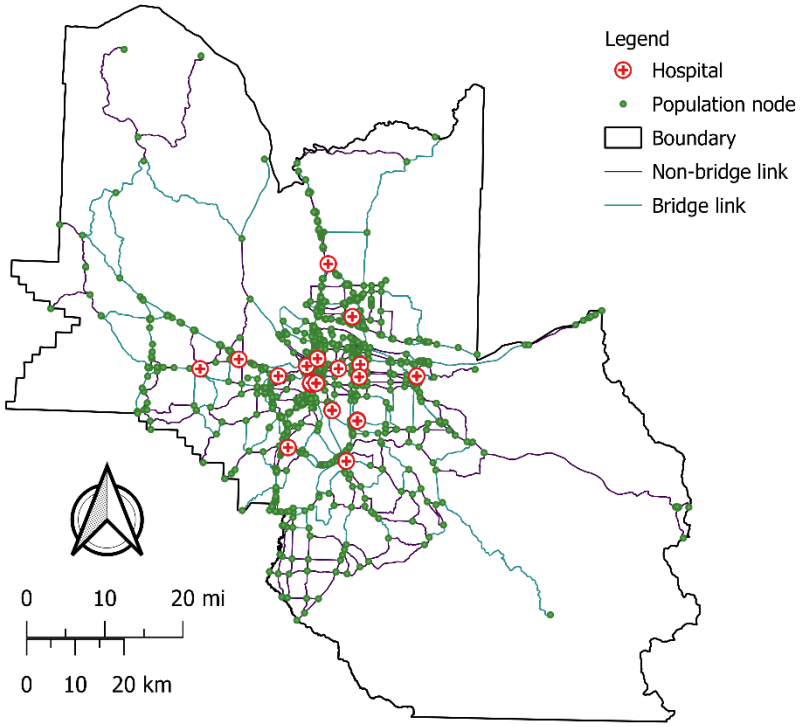

Source: FHWA

Figure 2.1. Illustration. Map of the Portland Metro Network.

2.2.2 Indicator for Network Accessibility

Accessibility-based performance indicators have been widely employed to quantify the functionality impact of network disruptions. These indicators evaluate how easily populations can reach essential services, particularly during emergencies. Several categories of accessibility measures exist in the literature. Methods such as the floating catchment area and the accessibility/remoteness index use binary thresholds to determine catchment areas around services, assuming full access within a fixed radius and none beyond (Luo and Wang, 2003; Taylor et al., 2006). More refined approaches, such as the enhanced two-step floating catchment area method (Luo and Qi, 2009), introduce stepwise distance decay functions and incorporate supply-demand balance. However, these methods suffer from limitations due to abrupt cutoffs and the subjective assignment of distance thresholds for accessibility calculation.

In this study, a simplified yet interpretable version of the Hansen integral accessibility index (Hansen, 1959) is adopted. The original Hansen index computes accessibility using a weighted sum of service opportunities discounted by distance. Here, identical service capacities are assumed for all the hospital nodes, and a reciprocal distance function is used. Specifically, the accessibility of a population node $i \in \mathcal{P}$ is the average of the reciprocal shortest-path distances to all hospital nodes, excluding itself if $i \in \mathcal{H}$. Mathematically, the accessibility of a population node i is given by:

$$A_i = \frac{1}{|\mathcal{H}_{\sim i}|} \sum_{j \in \mathcal{H}_{\sim i}} \frac{1}{d_{ij}}, \quad \forall i \in \mathcal{P}$$

Equation 2.2. Accessibility index of a population node *i*.

where d_{ij} = shortest distance between population node i to hospital node j, $\mathcal{H}_{\sim i}$ = set of hospital nodes excluding node i if it is also a hospital node. To evaluate network-level performance, the accessibility values of all population nodes are aggregated within the network, namely:

$$A_{NET} = \sum_{i \in \mathcal{P}} A_i$$

Equation 2.3. Accessibility index of a network.

This measure captures cumulative ease, with which the population can reach healthcare services. It is sensitive to increases in travel distance caused by infrastructure disruptions, particularly bridge failures, and reflects the functional consequences of these disruptions. It should be noted that the proposed accessibility index assumes equal "attractiveness" among all hospitals. Given more details about the hospitals (which are not available to the research team at the moment), the attractiveness of a hospital could be quantified, e.g., based on average waiting time (Ugwu et al., 2022), and incorporated into the accessibility index described herein.

2.2.3 Network Accessibility Risk

During and after a hazard event such as an earthquake, bridge failures can significantly reduce accessibility by increasing the travel distance between population nodes and hospital nodes. Therefore, the indirect risk of a transportation network can be calculated as the expected loss in accessibility, expressed as follows:

$$\rho_{NET} = \sum_{s} p(\boldsymbol{s}) \cdot \left| A_{NET,0} - A_{NET}(\boldsymbol{s}) \right|$$

Equation 2.4. Network accessibility risk.

where $\mathbf{s}$ = vector representing the survival/failure states of all bridge links in the network, $p(\mathbf{s})$ = probability of the system state, and $A_{NET}(\mathbf{s})$ and $A_{NET,0}$ = network accessibility values given a system state $\mathbf{s}$ and that without any bridge failure, respectively.

To compute these accessibility metrics given bridge failure, bridge fragility and detour data are integrated into the network model. Bridge characteristics are obtained from the FHWA's InfoBridge database (FHWA, 2024b), which provides parameters to determine fragility. Each bridge is associated with a detour length extracted from the FHWA InfoBridge database. It is assumed that this detour relies on local roads that are not represented in the adopted network model.

Since a single bridge link may contain multiple bridges, the failure probability of a bridge link is calculated by assuming independent failure of bridges on the link. To translate bridge failure probabilities into link failure probabilities, each bridge link is assumed to fail if any of its constituent bridges fail. Therefore, the failure probability of a bridge link l is computed as:

$$p_l = 1 - \prod_{i \in \mathcal{B}_l} (1 - p_i)$$

Equation 2.5. Failure probability of a corridor.

where $\mathcal{B}_\ell$ = the set of bridges located on link l, and p_i = the failure probability of bridge i. In addition, if a bridge link fails, the corresponding detour length is determined conservatively by adding detour lengths of all bridges on the link. As shortest-path distances increase due to detours, the resulting accessibility values decrease, thereby capturing the functional impact of bridge failures on healthcare access.

To estimate this risk efficiently, the Transitional Markov Chain Monte Carlo (TMCMC) approach as described in the Phase I report is applied herein. Originally developed for Bayesian updating, TMCMC is a sequential sampling method that can estimate the normalization constant (or evidence) of high-dimensional posterior distributions. In the context of risk assessment, the network risk can be formulated as the evidence term in Bayesian updating (Yang et al., 2024), thereby enabling the use of TMCMC for risk assessment.

Specifically, the TMCMC method initiates link failure samples from the prior distributions. A stage-by-stage sampling protocol sequentially samples link failures that are most relevant to quantifying the network risk. This includes rare but high-consequence system states, which conventional Monte Carlo simulation struggles with. As a result, TMCMC offers an efficient means to quantify indirect risk even in large and complex networks. In addition to estimating network risk, the link failure samples in the last stage can be used to measure asset importance. These importance measures of links can support targeted decision-making for risk mitigation, as elaborated later. For a detailed description of the methodology, the reader is referred to the Phase I report (Yang et al., 2024).

2.3 CSZ EARTHQUAKES AND BRIDGE FAILURE PROBABILITIES

2.3.1 Seismic Hazard

To characterize the seismic hazard, ground motion intensity measures are obtained from broadband synthetic seismogram simulations developed under the M9 Project, which simulates magnitude 9 CSZ earthquakes (Frankel et al., 2018; Wirth et al., 2018). This dataset includes 30 distinct rupture scenarios, each representing a plausible variation in slip distribution, rupture dynamics, and source location along the subduction interface. For each scenario, spectral acceleration values at multiple periods are provided over a spatial grid covering the Portland Metro Area.

Based on HAZUS Technical Manual (FEMA, 2020), the spectral acceleration at 1-second period (Sa-1s) is used as the intensity measure for evaluating bridge fragility and the associated probability of bridge failure. For each of the 30 simulation scenarios, a unique spatial field of Sa-1s is available in a gridded format. To obtain ground motion estimates at bridge locations, cubic spline interpolation is applied to the gridded Sa-1s values, producing a continuous surface from which site-specific Sa-1s values can be extracted for all bridges. Considering all 30 scenarios, each bridge is assigned 30 distinct Sa-1s values, one from each scenario. In the later section, a method will be presented to select the most critical scenarios among the 30 scenarios.

2.3.2 Bridge Fragility Models

This case study uses the fragility models prescribed in the HAZUS Technical Manual (FEMA, 2020), which remains widely used for regional bridge risk assessments. In this approach, each bridge is assigned to one of the 28 HAZUS bridge classes based on structural characteristics extracted from the FHWA InfoBridge database. Each class has an associated “standard” fragility curve that determines the probability of reaching or exceeding a given damage state as a function of Sa-1s based on the cumulative distribution function (CDF) of a lognormal distribution. These standard curves are parameterized by a median value and a dispersion factor. The median value of a standard curve is further modified to account for bridge-specific attributes such as skew angle, foundation type, and abutment behavior (FEMA, 2020). Among the four damage states considered in HAZUS, the complete damage state (or DS5) is used to differentiate functional and nonfunctional states of a bridge. Thereby, the bridge failure probability is quantified by the probability of damage exceeding DS5. Note that other DS can be used in lieu of DS5 to align with the agency management goals. Based on the HAZUS model, the Sa-1s value at each bridge is used as input of the complete damage fragility curve to compute the probability of bridge failure.

2.3.3 Scenario Selection

As described earlier, the ground motion dataset consists of 30 distinct CSZ earthquake scenarios, each with a plausible Sa-1s field. Because ground shaking intensity and spatial distribution vary across these scenarios, the expected damage and accessibility loss also differ among scenarios. To select the worst-case scenario for risk assessment, a selection approach is applied. Specifically, for each bridge, the failure probability is computed for all 30 scenarios using the HAZUS fragility curve described previously. The scenario that results in the highest failure probability is recorded for that bridge. The scenario that is recorded by a majority of all bridges is identified as the worst-case scenario. Following this procedure, the scenario labeled csz009 is selected from the 30 scenarios. Figure 2.2 shows the spatial distribution of Sa-1s field in this scenario. This scenario is then used in accessibility risk assessment.

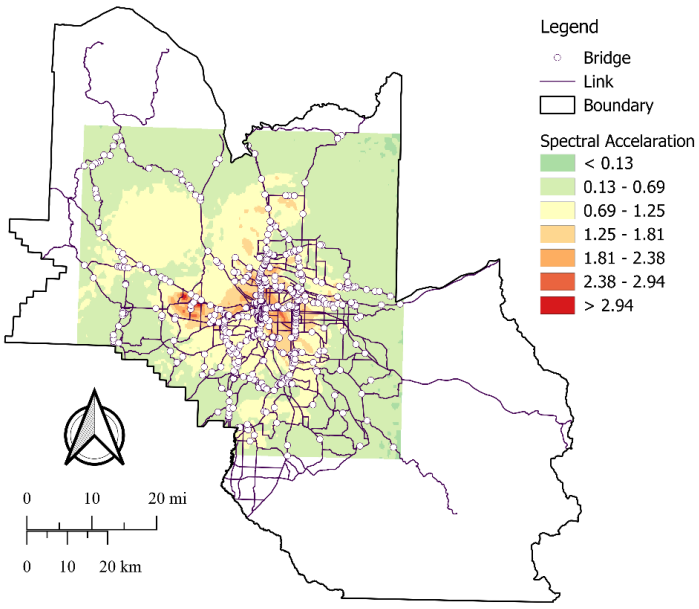

Source: FHWA

Figure 2.2. Illustration. Sa-1s field created for scenario csz009.

2.4 RESULTS FROM RISK ASSESSMENT

The indirect risk to hospital accessibility in the Portland Metro Area is evaluated using the TMCMC approach under the most detrimental CSZ earthquake scenario, selected based on the approach described above. The expected reduction in accessibility, quantified as network-level risk, is 11.6% based on the HAZUS fragility models.

In addition to estimating risk at system-level, the TMCMC samples are used to derive importance measures for each bridge link. Following the Phase I study, the risk-informed importance measure α_k of bridge link k is computed as:

$$\alpha_k = \frac{\sum_{j=1}^{N_s} s_{jk}^{(-1)}}{N_s}$$

Equation 2.6. Risk-informed importance measure of a corridor.

where N_s= number of TMCMC samples in the final stage, and $s_{jk}^{(-1)}$ = binary damage state of bridge link k in sample j. This measure corresponds to the posterior failure frequency of the asset and captures both likelihood and consequence in a single metric.

Bridge links with high importance values either have a high likelihood of failure, a great impact on accessibility, or both. These values support rational prioritization of assets retrofitting, as discussed in the later section. Figure 2.3 shows the spatial distribution of bridge link importance across the Portland network. The top-ranked bridge links are also summarized in Table 2.1. These high-importance links are concentrated along major corridors such as I-5, I-84, and I-405, reflecting both structural vulnerability and their central role in maintaining hospital access under seismic disruption.

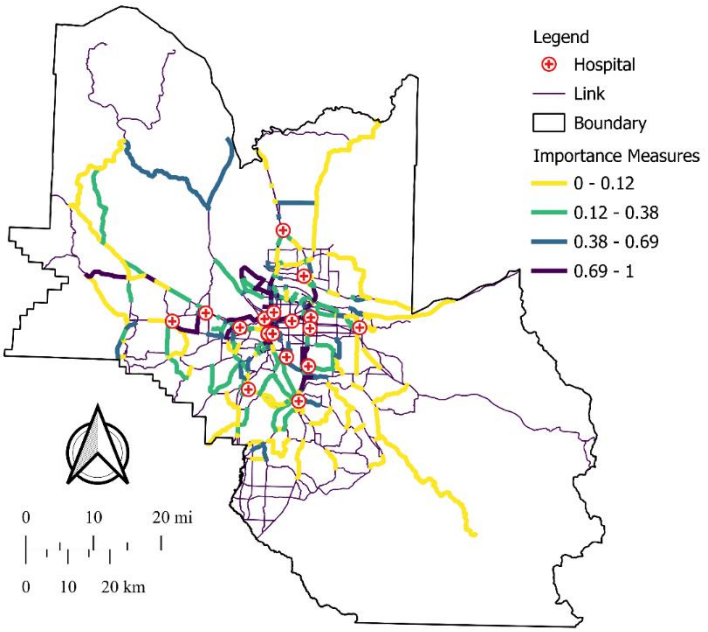

Source: FHWA

Figure 2.3. Illustration. Map of bridge link importance measures.

Table 2.1. Corridors with high risk-informed importance.

Rank	Link ID	Corridor Name
1	89	I-405 b/n Burnside St and SW Taylor St
2	124	I-5 b/n Burnside St and SE Washington St
3	170	NW Cornell Rd b/n NW Saltzman Rd and NW 23rd
4	78	I-405 between SW Clay St and SW Taylor St
5	118	I-84 b/n NE 39th Ave and NE 82nd Ave
6	100	I-84 b/n NE 16th Ave and NE Sandy Blvd
7	101	I-5 b/n SE Washington St and Morrison St
8	380	I-5 b/n N Marine Dr and Lewis and Clark Hwy
9	194	I-205 (Northbound) b/n SE Sunnyside Rd and SE Foster Rd
10	115	I-205 (Southbound) b/n SE Sunnyside Rd and SE Foster Rd

2.5 RISK-INFORMED RETROFIT PRIORITIZATION

In addition to knowing what corridor is more critical to the accessibility, it is also of practical importance to understand how sensitive the risk is to the reduction of bridge failure probabilities. With this information, the risk reduction measures can be prioritized. Compared to a full-fledged optimization, prioritization is more informative and actionable among decision-makers due to the following two reasons:

- The selection of projects based on prioritization can be easily understood by a decision-maker and communicated with other stakeholders. It can also be formatted into the common benefit-to-cost ratio (BCR) approach or incremental BCR (IBCR) approach. Both are commonly conducted within existing bridge management systems.

- By maintaining a prioritized list of projects, the programming is more robust to potential changes in the budget available. If more funding becomes available, additional projects can be simply added to the working order. Otherwise, projects can be triaged based on their BCR or IBCR. This relieves the analysts from conducting new optimization each time a budget constraint changes. It also avoids complications when optimization suggests removal already implemented projects when budget varies.

To illustrate this process, a corridor-based consequence measure for indirect risk with respect to the network accessibility is proposed using the following equations:

$$C_k = \frac{ln\, p_k}{ln\, \alpha_k}$$

Equation 2.7. Indirect failure consequence based on risk assessment results.

where C_k = indirect failure consequence; p_k = prior failure probability of link k, obtained from the bridge fragility model and Equation 2.5. Based on this measure, the benefit of retrofitting an asset can be determined as the reduction of asset-level risk expressed as follow:

$$B_{p,k} = \left(p_k - p_{p,k}\right) \cdot C_k v$$

Equation 2.8. Benefit of a retrofit project.

where $B_{p,k}$ = benefit of project p for link k; $p_{p,k}$ = reduced failure probability of link k due to project p; v = factor to convert unit of C_k to a monetary value.

For the case study network, one retrofit measure is assumed for each link. The effect of this retrofit measure is to reduce the seismic vulnerability of all bridges on the link. Specifically, given the retrofit measure, the HAZUS fragility curves based on the NBI data for all bridges on the link would be replaced with fragility curves with a median equal to 1.70g and a dispersion equal to 0.6, which corresponds to the most seismically reliable bridge class determined in the HAZUS model (FEMA, 2020). The cost of the retrofit measure is assumed based on the total deck area of all

bridges on the link. The cost per square-foot of deck area is assumed to be \$377/ft^2 (FHWA, 2025). The conversion factor v in Equation 2.8 is assumed to be the average value of all bridges estimated by deck areas. Note that the calculated BCR is sensitive to this conversion factor. Hence, the BCR should be considered as a relative measure to prioritize projects instead of their absolute return on investment.

Based on the discussion and assumptions above, Table 2.2 listed the top 20 links based on the highest benefit according to Equation 2.8 and the highest BCR, respectively. Comparing Table 2.2 and Table 2.1 reveals that the priorities based on the benefit or the BCR do not overlap with the risk-informed ranking of links. This is because the links in Table 2.1 have high failure probabilities that can't be effectively reduced by the retrofit measures. For instance, this could happen when a link is located in a region with high intensity measure and/or contains several bridges (e.g., four to five bridges). Additionally, the links with highest benefit do not always overlap with high BCR due to the high retrofit cost of some high- benefit links. Nonetheless, 5 out of the 20 links do overlap as highlighted in Table 2.2. Table 2.2 is directly applicable to select projects under budgetary constraints without running any optimization algorithms. In particular, the decision-maker may only run down the list based on BCR and the total budget. Detailed procedures can be found in the bridge management workshop workbook (FHWA, 2023)

Table 2.2. Link priorities based on indirect consequence and BCR.

Priority	Top links based on benefit	Benefit (risk reduction)	Top links based on BCR	BCR
1	101	2817241.4	**8**	278.60
2	118	1746191.3	289	216.97
3	**8**	1247226.5	305	160.74
4	100	965970.05	254	138.25
5	314	587723.48	363	122.74
6	155	573427.13	19	106.98
7	386	545383.98	223	105.19
8	170	534176.1	353	97.56
9	377	532951.83	149	96.38
10	124	525882.92	5	95.12
11	320	521919.51	260	94.95
12	177	520473.73	**283**	93.36
13	96	508159.83	25	91.67
14	**220**	501980.44	387	88.37
15	311	475582.78	**220**	80.22
16	236	473162.27	62	78.47
17	179	472993.04	**99**	74.11
18	**99**	449964.82	74	73.96
19	**283**	436427.33	**108**	72.30
20	**108**	426771.76	156	69.37

2.6 SUMMARY AND REMARKS

Focusing on the PDX bridge network and post-earthquake accessibility to hospitals, Case study II demonstrated the application of the TMCMC approach to indirect risk assessment based on network functionality. The results indicate that a major Cascadia Subduction Zone earthquake can

significantly reduce access to healthcare services. A practical approach was described to translate the risk assessment results into actionable retrofitting decisions. It should be noted that the results are based on several assumptions stated in the previous sections. Caution should be exercised when interpreting the results. Additionally, the optimality of the selected projects based on the described approach deserves more in-depth and systematic investigation in future studies.

CHAPTER 3

CONCLUSIONS

Based on the investigation in case study I, the following conclusions can be drawn:

- In order to capture the full range of hazard intensity, the USGS hazard model can be used for seismic risk assessment with the proposed approach. Different strategies are explored to reconstruct a hazard curve from the finite and discrete data of intensity levels and their annual probabilities of exceedance. It is found that for accurate risk assessment, the likelihoods of different intensity levels should be best evaluated using the interpolated cubic spline between the logarithmic annual rate of exceedance and the logarithmic IM value.
- For the determination of hazard scenarios, it is important to balance the accuracy for risk assessment and the practicality of the risk table. For the case study area, it is found that 10 hazard scenarios are sufficient to accurately estimate the seismic risk of high-risk bridges. The upper bound of the integration domain of the risk integral can affect the accuracy of the estimated risk. For seismic events, it has been empirically demonstrated that the largest intensity currently considered in the USGS hazard model is sufficient as the upper bound to accurately estimate the seismic risk of bridges. In practice, the sufficiency of an upper bound can be examined either (a) by ensuring that the complete damage probability under the upper bound intensity is sufficiently large or (b) through the incremental analysis using gradually raised upper bound, as detailed in case study I.

Based on the investigation in case study II, the following conclusions can be drawn:

- Compared to pre-earthquake performance, a magnitude 9 CSZ earthquake scenario may result in a 11.6% reduction in hospital accessibility across the Portland area network, measured in terms of the adapted Hansen accessibility index. This reflects a significant disruption in the ability of communities to reach healthcare services in the aftermath of a major earthquake.
- The TMCMC-based sampling approach provides an efficient means of evaluating network risk without exhaustively enumerating all possible failure combinations. It also yields risk-informed importance measures for each bridge link. The latter represent the contribution of the assets to the system-level accessibility loss. These measures offer a rational basis for retrofitting prioritization and resource allocation.

ACKNOWLEDGMENTS

The authors would like to acknowledge the support from Federal Highway Administration, especially from the technical point of contact of the project, Jia-Dzwan (Jerry) Shen. The help and valuable comments received from the members of the technical panel are also greatly appreciated. Panel members include Bert H. Hartman (ODOT), Albert Nako (ODOT), Derek Constable (FHWA), Derek Soden (FHWA), Elizabeth Habic (FHWA), Jeffrey Ger (FHWA), Kornel Kerenyi (FHWA), Robert Kafalenos (FHWA).

REFERENCES

Bradley, B.A., Dhakal, R.P., Cubrinovski, M., Mander, J.B., MacRae, G.A., 2007. Improved seismic hazard model with application to probabilistic seismic demand analysis. Earthq Engng Struct Dyn 36, 2211–2225. https://doi.org/10.1002/eqe.727

Cornell, C.A., Banon, H., Shakal, A.F., 1979. Seismic motion and response prediction alternatives. Earthquake Engineering & Structural Dynamics 7, 295–315. https://doi.org/10.1002/eqe.4290070402

DOGAMI, 2013. Oregon Seismic Hazard Database (OSHD), release 1.0 [WWW Document]. Oregon Department of Geology and Mineral Industries (DOGAMI). URL https://pubs.oregon.gov/dogami/dds/p-OSHD-1.htm (accessed 12.26.24).

Dong, Y., Frangopol, D.M., 2015. Risk and resilience assessment of bridges under mainshock and aftershocks incorporating uncertainties. Engineering Structures 83, 198–208. https://doi.org/10.1016/j.engstruct.2014.10.050

FEMA, 2020. HAZUS Earthquake Model Technical Manual (HAZUS v4.2 SP3). Federal Emergency Management Agency (FEMA), Washington, DC.

FHWA, 2025. Bridge Replacement Unit Costs 2023 [WWW Document]. FHWA Bridges & Structures. URL https://www.fhwa.dot.gov/bridge/nbi/sd2023.cfm#:~:text=National%20Average%20of%20the%20costs%20collected%20to,bridges%20is%20%24377%2Fft2 (accessed 11.19.25).

FHWA, 2024a. FHWA InfoBridge: Data [WWW Document]. Federal Highway Administration (FHWA) InfoHighway Website. URL https://infobridge.fhwa.dot.gov/Data (accessed 12.26.24).

FHWA, 2024b. Long-Term Bridge Performance (LTBP) InfoBridge [WWW Document]. Federal Highway Administration. URL https://infobridge.fhwa.dot.gov (accessed 1.1.25).

FHWA, 2023. Bridge Management Systems Workshop Participant Workbook [WWW Document]. URL https://www.fhwa.dot.gov/bridge/management/FHWA_BMS_workbook_1120.pdf (accessed 12.5.23).

Frankel, A., Wirth, E., Marafi, N., Vidale, J., Stephenson, W., 2018. Broadband Synthetic Seismograms for Magnitude 9 Earthquakes on the Cascadia Megathrust Based on 3D Simulations and Stochastic Synthetics, Part 1: Methodology and Overall Results. Bulletin of the Seismological Society of America 108, 2347–2369. https://doi.org/10.1785/0120180034

Géron, A., 2019. Hands-On Machine Learning with Scikit-Learn, Keras, and TensorFlow. O'Reilly Media, Inc., Sebastopol, CA.

Goodwin, P., Wright, G., 2014. Decision analysis for management judgment, Fifth edition. ed. Wiley, Chichester.
Hansen, W.G., 1959. How Accessibility Shapes Land Use. Journal of the American Institute of Planners 25, 73–76. https://doi.org/10.1080/01944365908978307
Keeney, R.L., Raiffa, H., 1993. Decisions with Multiple Objectives – Preferences and Value Tradeoffs. Cambridge University Press, Cambridge, UK.
Luo, W., Qi, Y., 2009. An enhanced two-step floating catchment area (E2SFCA) method for measuring spatial accessibility to primary care physicians. Health Place 15, 1100–1107. https://doi.org/10.1016/j.healthplace.2009.06.002
Luo, W., Wang, F., 2003. Measures of Spatial Accessibility to Health Care in a GIS Environment: Synthesis and a Case Study in the Chicago Region. Environ Plann B Plann Des 30, 865–884. https://doi.org/10.1068/b29120
NEHRP, 2020. NEHRP Recommended Seismic Provisions for New Buildings and Other Structures. Volume I: Part 1 Provisions, Part 2 Commentary. Building Seismic Safety Council, Washington, DC.
Oregon Metro, 2025. Regional Land Information System Open Database [WWW Document]. URL https://rlisdiscovery.oregonmetro.gov/ (accessed 1.7.25).
Padgett, J.E., Dennemann, K., Ghosh, J., 2010. Risk-based seismic life-cycle cost–benefit (LCC-B) analysis for bridge retrofit assessment. Structural Safety 32, 165–173. https://doi.org/10.1016/j.strusafe.2009.10.003
Rivera-Royero, D., Galindo, G., Jaller, M., Betancourt Reyes, J., 2022. Road network performance: A review on relevant concepts. Computers & Industrial Engineering 165, 107927. https://doi.org/10.1016/j.cie.2021.107927
Sewell, R.T., Toro, G.R., McGuire, R.K., 1991. Impact of ground motion characterisation on conservatism and variability in seismic risk estimates (No. NUREG/CR-6467). US Nuclear Regulatory Commission, Washington, DC.
Taylor, M., Somenahalli, S., D'Este, G., 2006. Application of Accessibility Based Methods for Vulnerability Analysis of Strategic Road Networks. Networks and Spatial Economics 6, 267–291. https://doi.org/10.1007/s11067-006-9284-9
Ugwu, I.A., Salarieh, B., Salman, A.M., Petnga, L., Williams, M., 2022. Postdisaster Recovery Planning for Interdependent Infrastructure Systems Prioritizing the Functionality of Healthcare Facilities. Journal of Infrastructure Systems 28, 04022038. https://doi.org/10.1061/(ASCE)IS.1943-555X.0000719
USGS, 2024. USGS Earthquake Hazard Toolbox [WWW Document]. United States Geological Survey (USGS). URL https://earthquake.usgs.gov/nshmp/ (accessed 12.26.24).
Wirth, E.A., Frankel, A.D., Marafi, N., Vidale, J.E., Stephenson, W.J., 2018. Broadband Synthetic Seismograms for Magnitude 9 Earthquakes on the Cascadia Megathrust Based on 3D Simulations and Stochastic Synthetics, Part 2: Rupture Parameters and Variability. Bulletin of the Seismological Society of America 108, 2370–2388. https://doi.org/10.1785/0120180029
Yang, D.Y., Khosravifar, A., Moug, D., Unnikrishnan, A., 2024. Framework and Methodology for Risk-Based Bridge and Tunnel Asset Management: Objective Risk Assessment and Network Level Evaluation (No. https://rosap.ntl.bts.gov/view/dot/79026). Portland State University, Portland, OR.